

Nonnuclear Experimental Capabilities to Support Design, Development, and Demonstration of Microreactors

P. Sabharwall, J. L. Hartvigsen, T. J. Morton, J. Yoo, S. Qin, M. Song, D. P. Guillen, T. Unruh, J. E. Hansel, J. Jackson, J. Gehin, H. Trellue, D. Mascarenas, R. S. Reid & C. M. Petrie

To cite this article: P. Sabharwall, J. L. Hartvigsen, T. J. Morton, J. Yoo, S. Qin, M. Song, D. P. Guillen, T. Unruh, J. E. Hansel, J. Jackson, J. Gehin, H. Trellue, D. Mascarenas, R. S. Reid & C. M. Petrie (2023) Nonnuclear Experimental Capabilities to Support Design, Development, and Demonstration of Microreactors, Nuclear Technology, 209:sup1, S41-S59, DOI: [10.1080/00295450.2022.2043087](https://doi.org/10.1080/00295450.2022.2043087)

To link to this article: <https://doi.org/10.1080/00295450.2022.2043087>



© 2022 The Author(s). Published with license by Taylor & Francis Group, LLC.



Published online: 18 Jun 2022.



[Submit your article to this journal](#)



Article views: 1597



[View related articles](#)



[View Crossmark data](#)



Citing articles: 1 [View citing articles](#)



Nonnuclear Experimental Capabilities to Support Design, Development, and Demonstration of Microreactors

P. Sabharwall,^{a*} J. L. Hartvigsen,^a T. J. Morton,^a J. Yoo,^a S. Qin,^a M. Song,^a D. P. Guillen,^a T. Unruh,^a J. E. Hansel,^a J. Jackson,^a J. Gehin,^a H. Trellue,^b D. Mascarenas,^b R. S. Reid,^b and C. M. Petrie^c

^aIdaho National Laboratory, Nuclear Systems Design and Analysis Division, 1955 N. Fremont Avenue, Idaho Falls, Idaho 83415

^bLos Alamos National Laboratory, Post Office Box 1663, Los Alamos, New Mexico 87545

^cOak Ridge National Laboratory, Nuclear Energy and Fuel Cycle Division, Post Office Box 2008, Oak Ridge, Tennessee 37831

Received August 23, 2021

Accepted for Publication February 7, 2022

Abstract — *This work provides a summary of selected experimental capabilities being developed to support nonnuclear testing and demonstration of technology in support of microreactors under the U.S. Department of Energy's (DOE's) Microreactor Program. Major capabilities include the Single Primary Heat Extraction and Removal Emulator (SPHERE) and the Microreactor Agile Non-nuclear Experimental Test Bed (MAGNET). The SPHERE facility allows for controlled testing of the steady-state and transient heat rejection capabilities of a single heat pipe using electrical heaters that simulate nuclear heating. The facility is capable of monitoring axial temperature profiles along the heat pipe and surrounding test articles during startup, steady-state operation, and transients. Instrumentation includes noncontact infrared thermal imaging, surface thermocouples, spatially distributed fiber optic temperature and strain sensors, electrical power meters, and a water-cooled, gas-gap calorimeter for quantifying heat rejection from the heat pipe. The facility can be operated under both vacuum and inert-gas conditions. The MAGNET facility is a large-scale, 250-kW electrically heated microreactor test bed to enable nonnuclear experimental evaluation of a variety of microreactor concepts. It can be supplied to electrically heat a scaled section of a microreactor and further test the capabilities of heat rejection systems. The initial MAGNET experiments will support technology maturation and reduce uncertainty and risk associated with the design, operation, and deployment of monolithic heat pipe-based reactors. However, this test bed can broadly be applied to multiple microreactor concepts to evaluate a wide range of thermal-hydraulic and structural phenomena such as interface coupling with power conversion units and other collocated systems. MAGNET can evaluate integral thermomechanical effects during electrical heating of an array of heat pipes in a larger test article. Examples of initial testing will include thermal stresses in the monolith and the impact of debonding of a heat pipe from the core block and how that failure could impact surrounding heat pipes, i.e., understanding the potential for cascading failure. This work also discusses some modeling capabilities that can support experiment design, analysis, and interpretation, including the heat pipe code Sockeye and a comparison of thermal-structural simulations performed using ABAQUS and STAR-CCM+.*

Keywords — *Microreactor; heat pipe-cooled reactors, advanced reactors, thermal hydraulics, advanced energy systems.*

Note — *Some figures may be in color only in the electronic version.*

*E-mail: piyush.sabharwall@inl.gov

This is an Open Access article distributed under the terms of the Creative Commons Attribution-NonCommercial-NoDerivatives License (<http://creativecommons.org/licenses/by-nc-nd/4.0/>), which permits non-commercial re-use, distribution, and reproduction in any medium, provided the original work is properly cited, and is not altered, transformed, or built upon in any way.

I. INTRODUCTION

There is an increasing need for more reliable and readily available energy in special purpose applications. A microreactor is designed for use in unique applications where energy generation on the order of megawatts is

needed, but otherwise unavailable or prohibitively expensive.¹ Possible applications include military installations, remote communities, industrial processes, and possible integration with hybrid energy systems and microgrids while providing potential load-following capabilities. Typical power needs in these use cases range from 1 to 10 MW(electric). In many current applications, power generation at this scale is achieved through the use of diesel generators. However, increasing costs, clean energy goals, and supply chain constraints have prompted a desire to examine other options to ensure energy availability and reliability. Microreactors generally produce less than 20 MW(thermal). They are factory manufactured, easily transported, and due to neutronic simplicity, allow for semi- or fully autonomous operation.² The use cases for generated energy may call for electricity production, direct use of process heat, or both. There are many types of microreactors being considered in the United States, but gas-cooled, molten-salt-cooled, and heat pipe-cooled reactors are the main designs being considered.^{1,3} These reactors operate in different thermal regimes; therefore, they allow for flexibility when selecting a reactor for a specific use case. Through ongoing efforts to ensure accelerated deployment, the U.S. Department of Energy (DOE) Microreactor Program (MRP) is working closely with vendors, the Nuclear Regulatory Commission (NRC), and other DOE programs to develop capabilities to demonstrate concept feasibility through nonnuclear testing. Once proven, these can assist with nuclear testing using the nuclear test bed Microreactor Applications Research Validation and Evaluation Project (MARVEL) (Ref. 2). Such testing will evaluate technical readiness levels for specific reactor concepts. These readiness-level evaluations can then be further used in conjunction with an expanded decision framework to define a path toward first-of-a-kind deployment.

To support the development of microreactor technology, Idaho National Laboratory (INL) is in the process of establishing a 250-kW electrically heated microreactor test bed to enable experimental evaluation of a variety of microreactor concepts. Major capabilities include the Microreactor Agile Non-nuclear Experimental Test Bed (MAGNET) facility being constructed at INL that will assist with the development, demonstration, and validation of microreactor components and systems. The purpose of the test bed is to support technology maturation that will reduce uncertainty and risk relative to the operation and deployment of this unique class of systems. The stakeholders for this test bed include microreactor developers, energy users, and regulators. Regulators can be

engaged early in the design and testing to expedite regulatory approval and licensing.

Within MAGNET, systems and components can be safely tested, providing valuable information on failure modes, operating regimes, and thresholds. The goal is to provide a test bed that is broadly applicable to multiple microreactor concepts. Various types of microreactors are being proposed, and these can be classified according to their core-cooling method: heat pipe, gas (pebble bed or prismatic), molten salt, or liquid-metal cooled. Each reactor type poses a different set of design and operational challenges, and the performance claims stated by commercial vendors have not been independently verified through rigorous testing. The initial set of tests to be performed in MAGNET are targeted toward demonstrating the feasibility and performance of heat pipe-cooled reactors because this concept is unique to very small nuclear reactors. However, the test bed will be constructed to accommodate other designs in addition to reactors cooled by heat pipes. INL is partnering with Los Alamos National Laboratory and Oak Ridge National Laboratory (ORNL) to meet the required development of testing and instrumentation needs.

The current work provides a summary of selected experimental capabilities and state-of-the-art instrumentation and sensors to obtain detailed maps of temperature and thermal strain. Additionally, a selection of modeling approaches is discussed that can support these experimental capabilities, including heat pipe models and thermal-structural analysis.

II. NONNUCLEAR TEST FACILITIES SUPPORTING VERIFICATION AND VALIDATION EFFORTS

The primary experimental hardware capabilities currently under development are focused on nonnuclear thermal and integrated systems testing and the development of test articles to perform experiments. Specifically, this includes the Single Primary Heat Extraction and Removal Emulator (SPHERE) and MAGNET. The capabilities described in this section will generate data that will further support other DOE programs and industrial needs. These data will be made available to researchers and developers for a range of testing purposes to support model development and verification and validation efforts.

II.A. Single Primary Heat Extraction and Removal Emulator

A process flow diagram for the SPHERE facility is shown in Fig. 1. Cooling water is recirculated using a 2.5-kW circulating chiller unit. The water flow loop

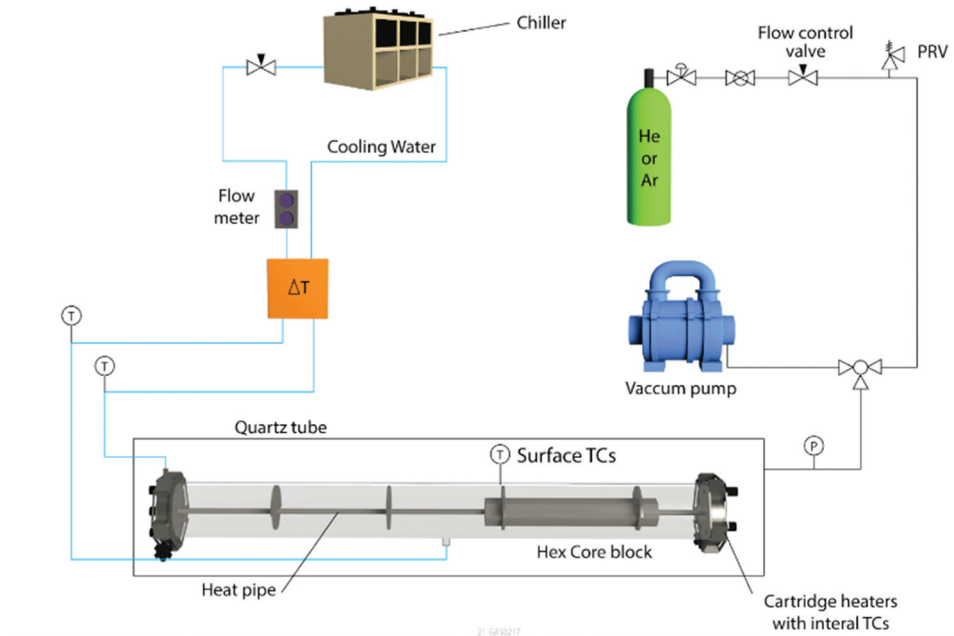


Fig. 1. Process flow diagram for the single-heat-pipe experiment facility (known as SPHERE).

includes a precision turbine flow meter and a delta-T meter that will allow for accurate determination of the heat removal rate from the heat pipe to the cooling water. Prior to testing, the quartz tube is evacuated using a vacuum pump and then backfilled with inert gas (either He or Ar). This process is repeated several times (by successive dilution) at the beginning of each test to ensure that all the air has been removed. An oxygen sensor provides a second validation of total removal of air from the system.

The objectives of the single heat pipe testing include⁴:

1. Document heat pipe thermal performance under a wide range of heating values and operating temperatures.
2. Observe heat pipe startup and transient operation.
3. Develop effective thermal-coupling methods between the heat pipe's outer surface and the core block and between the cartridge heaters and the core block.

Measurement of heat pipe axial temperature profiles during startup, steady-state, and transient operation involves using thermal imaging and surface temperature measurements, performing calorimetric measurements with a water-cooled gas-gap calorimeter, determining heat pipe operational limits, and testing under both vacuum and inert-gas conditions.⁴

The thermal performance of the operating heat pipes will be determined by the measurement of heat pipe heat removal capacity as a function of operating temperature. The heat removal rate is equal to the total heater power input, measured by power meters, minus any heat losses as determined by a combination of direct measurement by calorimetry measurements and analysis of temperature gradients through the block and along the heat pipe. The body of these heat pipes is stainless steel. The working fluid is sodium, and the wick structure is specific to the supplier. The total quantity of sodium in each heat pipe is small, roughly 60 to 80 g. After charging, the heat pipes are welded shut. From the standpoint of our operations, the heat pipes are fully closed, fully sealed test articles. As noted previously, the vapor pressure inside the heat pipes will be subatmospheric, even at their highest operating temperature, so any failure of the heat pipe would not involve a pressurized release of material. The design basis surface heat flux value for the cartridge heaters is 3.8 W/cm² based on expected microreactor core power densities. For the 6-in. block, this power density yields 317 W per heater and a total power of 1891 W. For the .5-m block with the same power densities, each heater would operate at 1 kW for a total power of 6 kW. For the 1-m block, each heater would operate at 2 kW for a total power of 12 kW. During testing in SPHERE, the heat fluxes that can be applied will be limited by the heat transfer rating of the heat pipes. This limitation will result in the use of significantly lower heat fluxes than the full prototypical core design values, especially for the longer core blocks. Heater operating temperatures will be limited to

750°C. Note that the vapor pressure of sodium is still well below 1 atm at this temperature. Therefore, the overpressurization failure of the heat pipe is not a concern. The single-heat-pipe experiments will be performed using a seven-hole hexagonal core block with the cross-sectional geometry shown in Fig. 2a. The core block material is stainless steel 316L. Three different core block lengths have been fabricated: 6 in., .5 m, and 1 m. A photograph of one of the hex blocks is presented in Fig. 2b. The outer ring of six holes in the core block will be fitted with cartridge heaters designed to mimic heating from microreactor fuel rods, and the center hole will be occupied by the heat pipe. The gaps between the heat pipe, heaters, and the hex block are filled with boron nitride (BN) paste to ensure a perfect thermal contact during the experiments.

Single-heat-pipe testing is performed in an inert-gas environment consisting of either helium or a helium-argon mixture, using a test fixture similar to the one shown in Fig. 3. The heat pipe assembly is housed in a cylindrical inert-gas environment formed by a quartz tube with flanges on either end that include fittings for inlet and outlet gas flows as well as feedthroughs for instrumentation and power. The quartz tube allows for visual observation of heat pipe

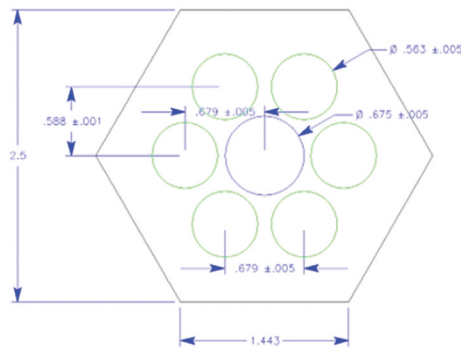
operation and quantitative thermal imaging. It also provides containment in the unlikely event of a leak of sodium from the heat pipe. A photograph of the quartz tube showing one of the end flanges and several internal Macor supports is presented in Fig. 4. The Macor supports are designed to hold the hexagonal core block and the heat pipe centered in the quartz tube. Macor was selected based on its low thermal conductivity and high allowable operating temperature, plus the fact that it is machinable.

The SPHERE test bed is currently in final assembly at INL (Fig. 4). The major characteristics of the test bed can be summarized as follows⁴:

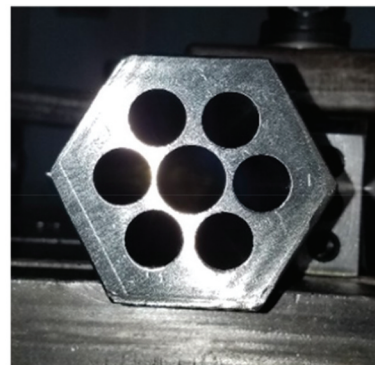
1. vacuum (10^{-4} torr) or inert gas
2. 8-ft-long × 6-in.-diameter quartz tube
3. flanges for gas flow connections and instrumentation feedthrough ports.

Electrical heating capability requires

1. a test bed designed for up to 20 kW electrical power to heaters
2. maximum test article temperature of 750°C



(a)



(b)

Fig. 2. (a) Cross-section geometry of core block for single-heat-pipe experiments and (b) photograph of seven-hole hex block end face in fabrication.

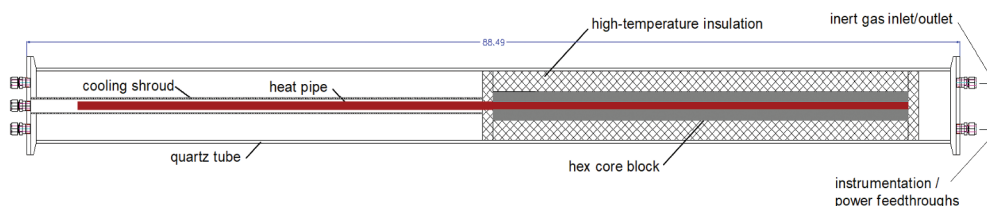


Fig. 3. Single-heat-pipe test fixture.

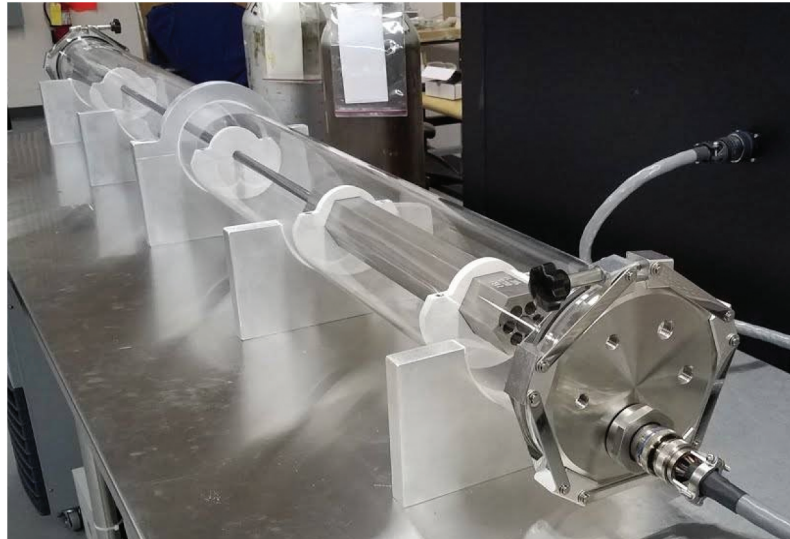


Fig. 4. Single-heat-pipe experiment quartz tube with core block, end flange, and Macor supports.

3. heat rejection through passive radiation or coupled with a water-cooled gas-gap calorimeter.

II.B. Microreactor Agile Non-nuclear Experimental Test Bed

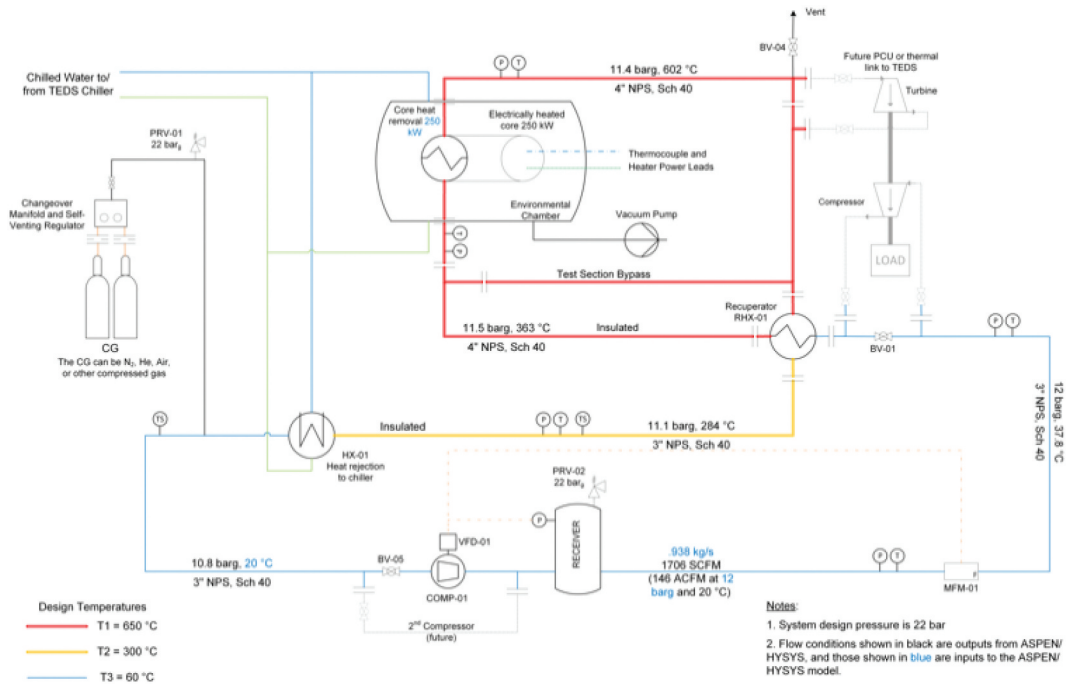
To support the development of microreactor technology, INL has established a 250-kW electrically heated microreactor test bed to enable experimental evaluation of a variety of microreactor concepts. MAGNET was constructed at INL to assist in the development, demonstration, and validation of microreactor components and systems. The purpose of this test bed is to support technology maturation that will reduce uncertainty and risk relative to the operation and deployment of this unique class of systems. However, the test bed will be constructed to accommodate other designs in addition to heat pipe-cooled reactors.

MAGNET was constructed at INL with the following objectives and technical goals:

1. Provide displacement and temperature data that could be used to verify potential design performance and to validate accompanying analytical models.
2. Show structural integrity of core structures: thermal stress, strain, aging/fatigue, creep, and deformation.
3. Evaluate the interface between the heat pipes and heat exchanger for both geometric compatibility, heat pipe functionality, and heat transfer capabilities.
4. Develop potential high-performance integral heat exchangers based on advanced manufacturing

techniques, incorporating high-efficiency heat transfer from the heat pipes or gas working fluid to the power conversion units (PCUs).

5. Test the interface between the heat exchanger and integrated systems for power generation or process heat applications.
6. Test microreactor components, such as gas circulators, control drums, or heat sinks.
7. Demonstrate the applicability of advanced fabrication techniques, such as additive manufacturing or diffusion bonding, to nuclear reactor applications.
8. Identify and develop advanced sensors and power conversion equipment, including instrumentation for autonomous operation.
9. Test waste heat recovery systems designed to increase system efficiency and improve economics.
10. Study cyclic loading and simulated reactivity feedback.
11. Enhance readiness of the public stakeholders, particularly DOE laboratories and the NRC, to design, operate, and test new types of high-temperature reactor components.
12. Capture data relevant to the development of autonomous microreactor structural integrity monitoring systems [e.g., digital image correlation (DIC)]. Use the data to develop and verify models and systems for system integrity monitoring.



(a)



(b)

Fig. 5. (a) MAGNET process flow diagram and (b) environmental enclosure.

A process flow diagram of MAGNET and a graphic of the MAGNET environmental chamber are shown in Fig. 5. Design specifications for MAGNET are shown in Table I.

In order to provide capabilities for integrated power conversion testing, a modified, commercially available Capstone C30 microturbine unit⁵ has been acquired (Fig. 6) and will be integrated with

TABLE I
MAGNET Design Specifications

Parameter	Value
Chamber size	5 × 5 × 10 ft
Heat removal	Liquid-cooled chamber walls, gas flow
Coolants	Air, inert gas (He, N ₂)
Gas flow rates	Up to 43.7 ACFM ^a at 290 psig
Design pressure	22 barg
Maximum power	250 kW
Maximum temperature	750°C
Heat removal	Passive radiation or water-cooled gas-gap calorimeter

^aACFM = actual cubic feet per minute.

MAGNET. Figure 6 shows the key components of the PCU, including the compressor, turbine, alternator, internal recuperator, gas cooler, and power management and distribution (PMAD) subsystem. Power generated can be fed to the electrical heaters in MAGNET to supplement externally supplied electricity or to a load bank as part of the co-located Microgrid Research Laboratory. The cycle is completely closed, and gas flows through the compressor and recuperator into the heat source heat exchanger, into the turbine, back into the recuperator, and finally into the gas cooler for the rejection of waste heat.

The C30 recuperator is an annular gas-gas heat exchanger that is physically integrated within the PCU housing whereas the heat source heat exchanger can be a gas-gas or liquid-gas heat exchanger, depending on reactor design. This PCU has been modified to use electrical heating⁶ rather than fossil-fuel combustion to provide a maximum power output of ~30 kW(electric) in a closed Brayton cycle (CBC) loop with nitrogen as the working fluid. A detailed

description of the PCU and the integration into MAGNET is given in Ref. 7. A proposed set of tests of the power control schemes and heat source/PCU coupling are outlined in Ref. 8.

II.B.1. PCU Integration into MAGNET

A modified commercial Capstone C30 microturbine is being integrated into MAGNET to enable performance evaluation of microreactor design concepts. The C30 PCU has been modified from an initial configuration that was reliant upon combustion heating to accept external electrical heating to simulate nuclear heat. This unit is well suited to coupled testing with a 75-kW(thermal) electrically heated heat pipe test article that provides a turbine inlet temperature of 600°C. Coupling various types of test articles with an actual power conversion system in the test bed will provide important feedback for technology maturation of microreactor components. The CBC PCU can operate over a range of steady-state and transient conditions to evaluate test article heat transfer performance in representative operational scenarios. A proposed set of tests of the power control schemes and heat source/PCU coupling are outlined by Guillen and Wendt.⁸

The MAGNET facility with the C30 offers a unique capability for testing microreactor components that is not available elsewhere. The test bed provides an opportunity for operator training on a small PCU by providing the ability to interface with the controls and obtain feedback on certain aspects of a microreactor integrated with a PCU CBC. Tests will be conducted to provide detailed reactor core and heat removal section thermal-hydraulic performance data for prototypical geometries and operating conditions and to demonstrate integration with relevant PCUs.

Possible future studies include the construction of a digital twin to facilitate further understanding of the

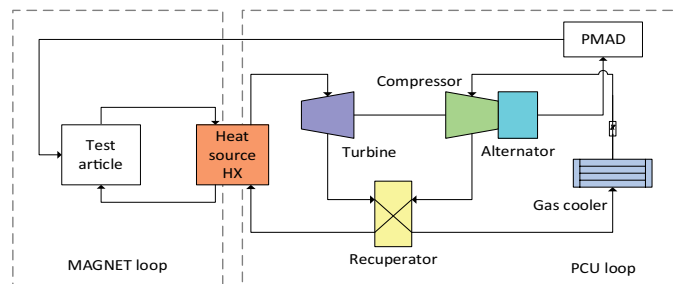


Fig. 6. Layout of PCU loop connected to the MAGNET loop by the heat source heat exchanger (HX = heat exchanger).

interaction between the simulated microreactor and the PCU.

The digital twin will be a system that includes a digital representation and simulation of a physical asset and utilizes machine learning and artificial intelligence to analyze data from the asset and simulation to determine trends, faults, or anomalies. Further, this twin will be developed through integration of Deep Lynx (a data warehouse technology), the Multiphysics Object-Oriented Simulation Environment (MOOSE), physical asset sensors, and physical asset controls. This work is novel because it will forward research regarding how to best integrate these software systems with physical sensors and asset controls.

Experimental data from coupled system operation could be valuable in developing and validating anomaly detection algorithms to facilitate remote or autonomous operations. It is recommended that a dynamic system model be developed to further investigate the transient operation (e.g., response times, system performance, control system parameters) of the coupled heat source/PCU system.

III. MODELING AND ANALYSIS TO SUPPORT EXPERIMENTS

Modeling and simulation can serve to provide relevant insights throughout the entire experimental procedure, from design to experimental data analysis (for physics not directly captured by experiments) to measurement planning. In this regard, the DOE MRP supports modeling and simulation activities for experiments at the SPHERE and MAGNET facilities, respectively, with the aim of producing high-fidelity experimental data. Given that the INL MOOSE-based heat pipe modeling software, Sockeye, is

still in development, the current heat pipe modeling and simulation effort focuses on leveraging commercial software packages. The major concerns of the single-heat-pipe experiment include the thermal behavior of the sodium heat pipe starting from a frozen state, heat pipe performance limits, and the resulting behavior of the heat pipe-cooled system. Another important aspect that should be well understood through this experimental effort is the potential concern from thermal stress across the structural materials in the high-temperature operating conditions of microreactors. In order to effectively achieve these goals and support the production of high-quality experimental data, modeling and analysis efforts for heat pipe startup and thermal stress induced in the hex block are conducted and summarized in this study.

III.A. Heat Pipe Startup Modeling

Among the major concerns of the single-heat-pipe experiment at INL are to understand the thermal behavior of the liquid-metal heat pipe starting from its frozen state and the associated heat pipe performance limits. To guide relevant validation data production while supporting preliminary insight into the current heat pipe experiment at the SPHERE facility, heat pipe modeling and analysis efforts are currently underway.

Recently, a simplified method to effectively analyze the frozen startup behavior of liquid-metal heat pipes has been proposed and tested. In this approach, the entire startup process of the liquid-metal heat pipes, including the melting of the working fluid (i.e., the liquid metal), transition of the vapor flow regime, and growth of continuum vapor flow along a heat pipe, is represented based solely on heat conduction equations. The key to this model development is to derive effective thermal conductivity of the gaseous phase of a working fluid during startup by

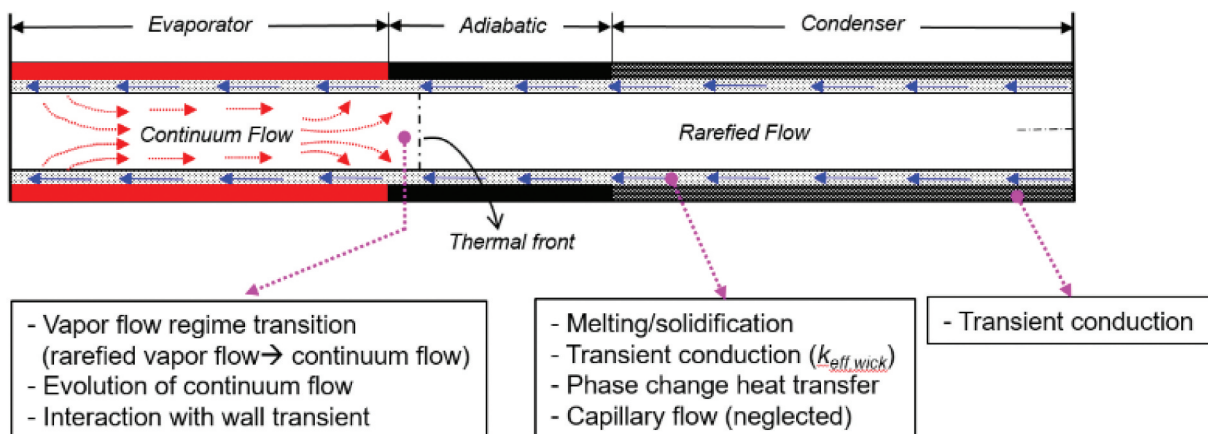


Fig. 7. Relevant heat pipe physics addressed in the simplified conduction-based heat pipe frozen startup analysis model.

employing appropriate simplifying physical assumptions and numerical methods. Figure 7 shows a set of relevant physics addressed in this conduction-based modeling approach to simulate the frozen startup behavior of the liquid-metal heat pipes. Given the substantial amount of work associated with this model development effort, readers are advised to see Refs. 9 and 10 for details on the physical assumptions, numerical method, mathematical formulations, and overall model-derivation processes.

The performance of the conduction-based heat pipe startup analysis model has been assessed using the transient heat conduction solver available in the commercial computational fluid dynamics tool STAR-CCM+ (version 15.06). Only heat conduction equations were solved for the different regions of a heat pipe (i.e., wall, wick, and vapor core) as a conjugate problem to simulate the entire process of the heat pipe's startup from frozen state. Figure 8 shows an example of comparison cases obtained from the recent model validation study, presenting that the conduction-based model predicts the startup thermal behavior of the sodium heat pipe observed by Faghri et al.¹¹ reasonably well.

The performance of the conduction-based model is currently being assessed using more liquid-metal heat pipe experimental startup data obtained from different research groups, and this modeling effort will be used to support INL's ongoing validation effort with single-heat-pipe experiments (i.e., seven-hole core block test) at the SPHERE facility and to guide the test plans.

III.B. Heat Pipe Post-startup Modeling

A heat pipe device is designed to reliably achieve a certain performance in terms of heat throughput over a range of operating temperatures. After the startup phase, the heat pipe can sustain a relatively high heat throughput; however, various limitations need to be considered to accurately predict heat transfer through a heat pipe. To account for these limits, they must either be achieved mechanistically by a flow model or expressions of these limits must be approximated analytically in some manner.

The heat pipe code Sockeye offers transient simulation capabilities that can be used to support experimental design and analysis. Sockeye's simulation capabilities can be classified into two approaches: a one-dimensional (1D), two-phase, compressible flow solution, and a two-dimensional (2D) effective heat conduction solution. The former is designed to mechanistically achieve the various operating limits in the confines of a computationally tractable 1D simulation, and the latter is designed to be a simple and numerically robust 2D simulation. Both approaches have utility, and analyses can use both in conjunction to achieve a holistic solution. In this section, some demonstrations of Sockeye's simulation capabilities are made.

The 1D flow model solves a well posed system of seven partial differential equations corresponding to conservation of mass, momentum, and energy in

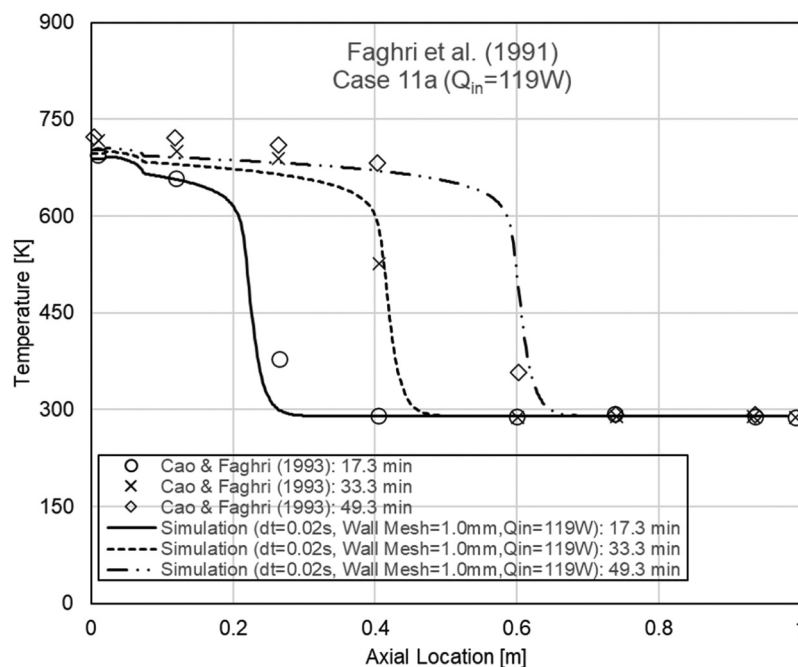


Fig. 8. Example of heat pipe wall temperature predictions compared against Cao and Faghri's¹² sodium heat pipe startup experiment.

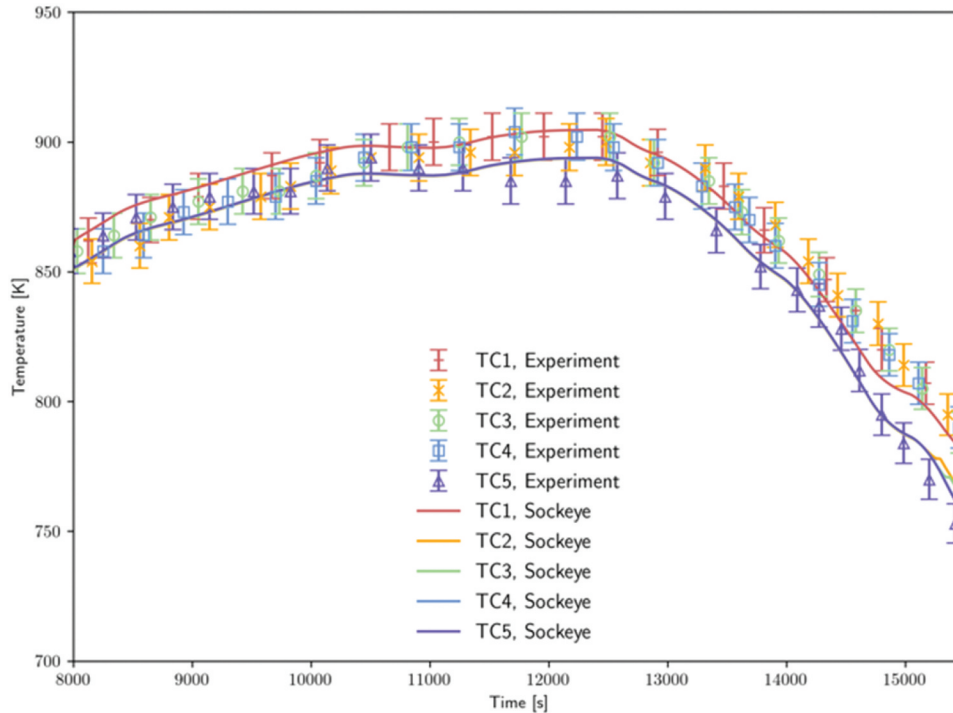


Fig. 9. Comparison of Sockeye's 1D flow model temperature solution to experimental data for the SAFE-30 heat pipe module test adopted from Ref. 13.

both phases, as well as a volume fraction evolution equation. This model is described with details in Ref. 13. Figure 9 shows temperature results from this model compared to thermocouple data for the SAFE-30 heat pipe module test,¹⁴ where error bars denote the listed uncertainty range for Type C thermocouples. In this test, a sodium heat pipe was oriented horizontally and heated with cartridge heaters and passively cooled via radiative losses. The simulation was started after the heat pipe was noted to be fully melted because this model is not yet suitable for startup transients. The 1D flow model was coupled to 2D heat conduction in the heat pipe wall, and the cartridge heater's power history was applied via a uniform heat flux in the evaporator region.

The 2D effective heat conduction model solves the heat conduction equation using representative thermal properties for three radial regions of the heat pipe: the cladding, the wick/liquid annulus, and the vapor core. In the vapor core, the efficient heat transport rate via convection is approximated with heat conduction with a very high thermal conductivity. When a heat pipe is operating without hitting any of its operational limits, these approximations are generally reasonable to capture heat transfer transients.¹³ However, when operation is subject to limitations, some account of these

effects must be considered. Figure 10 shows the results of a test problem demonstrating a cascading heat pipe failure. In the transient, for the first 200 s the heat pipe is heated at some power. At 200 s the power is increased to simulate the failure of an adjacent heat pipe and its share of the failed heat pipe power. At 400 s an adjacent heat pipe is failed, increasing power again. Various operational limits are evaluated using analytic approximations at a solution temperature. The heat rate at the condenser end is adjusted when the nominal heat rate through that boundary exceeds a given limit. The viscous and sonic limits are treated as recoverable, limiting the heat rate temporarily and causing the heat pipe to heat until those limits rise enough to no longer maintain limits. In contrast, the capillary limit is treated as a catastrophic limit requiring intervention; dryout is assumed to occur immediately. In the first third of the transient, the heat pipe temperature follows the viscous and sonic limit curves until they are no longer limiting, eventually approaching a steady state. Failure of one adjacent heat pipe leads to an adjustment toward another steady state. Finally, failure of an additional adjacent heat pipe is unsustainable; the power reaches the capillary limit, causing failure of the simulated heat pipe and demonstrating a cascading heat pipe failure.

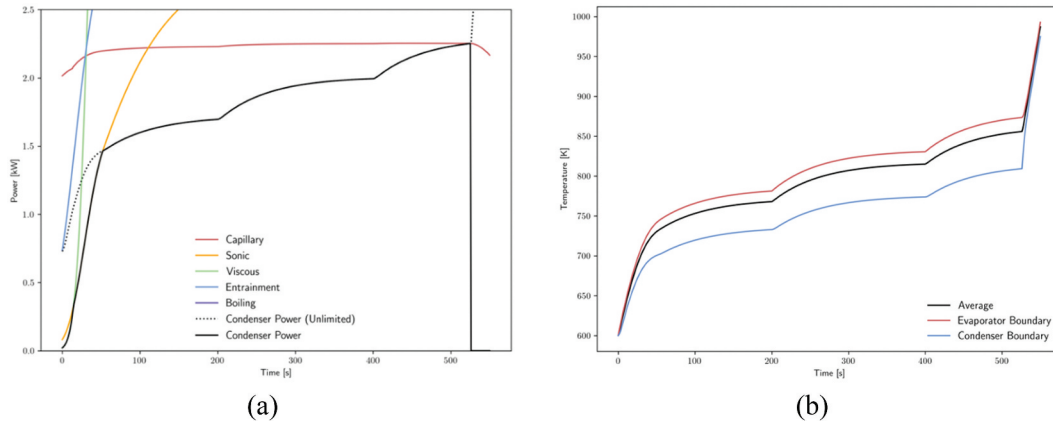


Fig. 10. Demonstration of Sockeye's 2D effective heat conduction model on a heat pipe cascading failure test problem showing (a) power vs. time and (b) temperature vs. time.

III.C. Coupled Thermal-Structural Modeling and Code-to-Code Benchmark

Another potential concern with the heat pipe-cooled microreactor is the large temperature gradient that occurs in the monolithic hex block during the heating/cooling stage; a larger temperature gradient would induce greater thermal stresses. The finite element method (FEM)-based software ABAQUS has been widely used and accepted in the structural analysis field. However, ABAQUS does have some limitations when dealing with multiphysics transient simulations, for example, the startup/shutdown process of heat pipes. On the other hand, as a professional high-fidelity computational fluid dynamics code, STAR-CCM+ has also developed its FEM-based solid stress solver code (since version 10.04) but more information is needed to gain further confidence. Therefore, using the ABAQUS FEM results as a reference, the benchmark study is performed to verify the FEM solver implemented in STAR-CCM+ and ultimately expand the stress analysis capability to utilize STAR-CCM+ for more complex heat pipe transient simulations.

To support the MRP and analyze the ongoing experimental work at INL, ABAQUS and STAR-CCM+ have been used to perform code-to-code comparisons with both the temperature profiles and stress distributions for the single-heat-pipe experiments. The FEM solver was used in both software simulations to estimate the temperatures and resultant thermal stresses that the seven-hole core block in the SPHERE facility might experience during testing. Coupled thermal-structural analysis for the heat pipe benchmark testing presented in this paper can help to provide insights into the heat transfer mechanics of high-

temperature heat pipe experiments as well as the structural integrity of the experimental design aspects.

III.C.1. Modeling Method and Setup

As for the modeling strategy, computational analyses with ABAQUS and STAR-CCM+ have been completed with a one-way coupling method; this means that the temperature distribution is solved with the heat transfer analysis first, subsequently using the temperature profile from the thermal-analysis step as the boundary conditions and starting the stress analysis step using the same computational domain as the model setup. An FEM solver is triggered for both heat transfer and stress analyses using ABAQUS and STAR-CCM+.

As shown in Fig. 2, the detailed hex block geometry is implemented in the coupled thermal-structural model; a single heat pipe is inserted in the central hole of the block, surrounded by six cartridge heaters to simulate fuel rod heating. STAR-CCM+ (version 15.06) was used to simulate the thermal stress behavior in the hex block. The program of version 15 provides the capability to calculate stress fields with FEM analysis. In the meantime, ABAQUS 2018.HF3 was also used to perform code-to-code benchmark thermal and structural simulations on INL's Falcon high-performance computing system. Dimensions were taken from previous reports^{15,16} for the case with a 152.4-mm-long hex block and cartridge heaters. Some important dimensions are summarized as follows:

1. *heat pipe*: 15.88 mm outer diameter (o.d.) × 14.45 mm inner diameter

2. center hex block hole diameter: 17.15 mm
3. diameter of six holes containing cartridge heaters: 14.30 mm
4. cartridge heater: 12.70 mm o.d.

Quarter symmetry is assumed, and one quarter of the hex block is modeled for the coupled temperature structural analysis. The bottom of the model is set to be fixed (constrained not to move axially) while the plane symmetry is applied to the two side surfaces for the quarter hex block model shown in Fig. 11. The inner surface of the heat pipe is fixed at a constant temperature of 650°C while the whole model is assumed to have an initial temperature of 20°C. As for the heating process, the total applied heat load was parametrically varied up to a maximum of 1902 W (317 W per cartridge heater). The cartridge heaters were modeled as monolithic 304 stainless steel with uniform volumetric heating, and the hex block and the heat pipe sheath were also modeled using 304 stainless steel. The cartridge-heater-to-hex-block gaps and the hex-block-to-heat-pipe gap were assumed to be filled by BN paste to ensure a perfect thermal contact during the whole experiment period. The BN paste is not included in the structural analyses currently, but this expansion phenomenon of BN will be investigated in a future study. The structural simulations included only elastic deformation with no consideration of creep or plasticity in the model. Radial heat losses to the quartz tube and axial heat losses besides heat transferred to the heat pipe were not included. More detailed material properties and the model setup can be found in Yoo et al.,¹⁰ Petrie and Ezell,¹⁶ and Qin et al.¹⁷

Uniform hexahedral meshes were applied to the model geometry for both ABAQUS and STAR-CCM+. With the consideration of the simulation accuracy and

computational cost, a uniform 1-mm hexahedral mesh base size was used for all the coupled temperature structural simulations with both software, as shown in Fig. 12.

III.C.2. Results and Discussion

Figures 13 and 14 show the temperature distributions as well as the Von Mises stress contour plots in the hex block with both a top and side view using ABAQUS (Figs. 13a, 13b, 14a, and 14b) and STAR-CCM+ (Figs. 13c, 13d, 14c, and 14d). The maximum temperature is located on the outer surface of the hex block due to the adiabatic setting of the model, while maximum stress in the hex block happens at the inner surface of the heat pipe hole. As expected, the outstanding thermal stress at this area is mainly caused by the temperature gradient between the heater and the heat pipe.

The Von Mises stress distribution contour shows that the maximum stress is located along the path between the centers of the heat pipe and channel heaters, as shown in Fig. 15. As shown in Fig. 13, the large temperature gradient at the shortest path results in large stresses. This result shows that the pitch thickness between the heat pipe and channel heaters could be an important parameter for determining maximum thermal stress in the hex block; considering the heat conduction, the pitch length could be optimized by varying the diameter of the heat pipe and cartridge as well as the thickness of the BN paste between the hex block and components. Given the same heat flux rate from the channel heaters, according to Fourier’s law, increasing the pitch would be helpful in decreasing this temperature gradient. The parametric study for the pitch between holes, considering the manufacturing processes, should be examined in the future.

The parametric study for the coupled temperature displacement analyses was performed in this report by

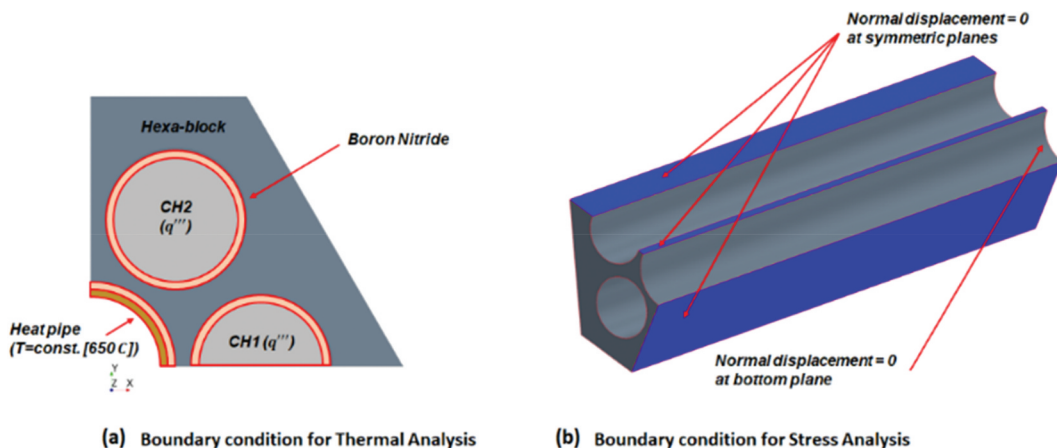


Fig. 11. Boundary conditions for (a) thermal analysis and (b) stress analysis.

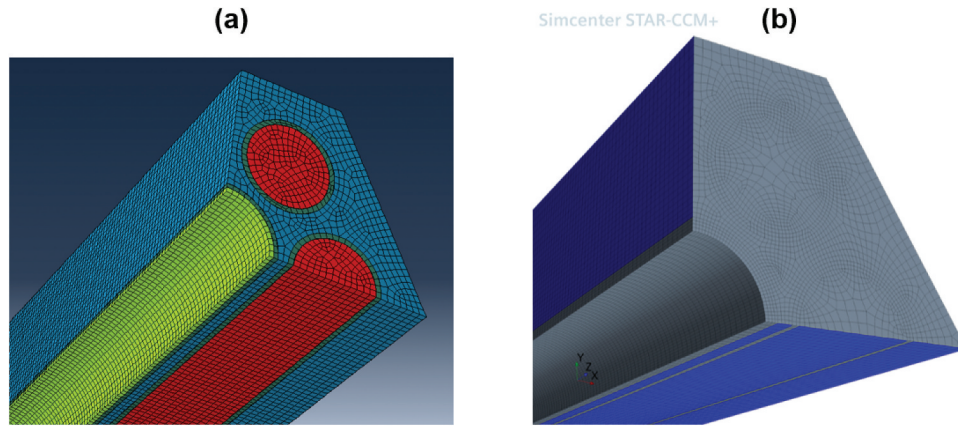


Fig. 12. Mesh structure of test case (quarter block): (a) ABAQUS and (b) STAR-CCM+.

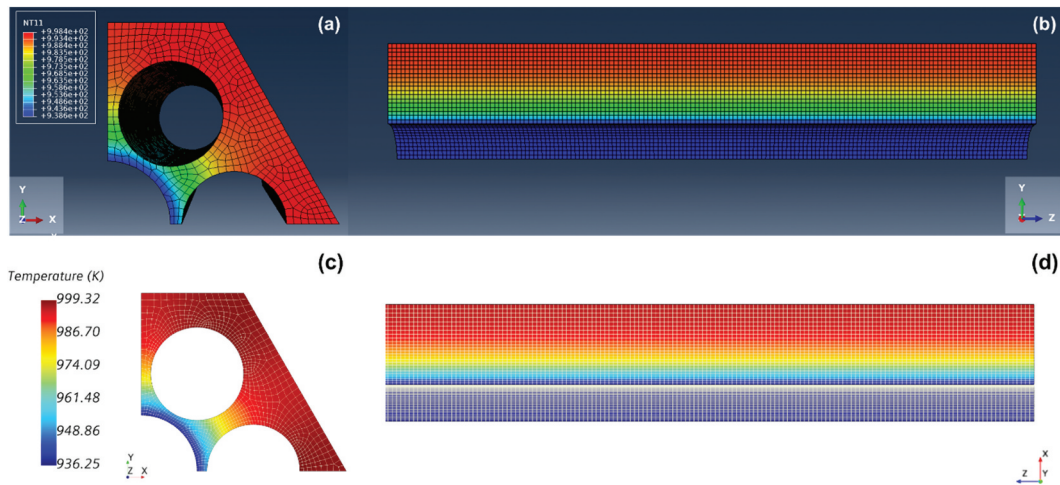


Fig. 13. Temperature distribution with the heating power of 317 W per cartridge heater at the (left) top and (right) side view of the hex block [(a) ABAQUS and (b) STAR-CCM+].

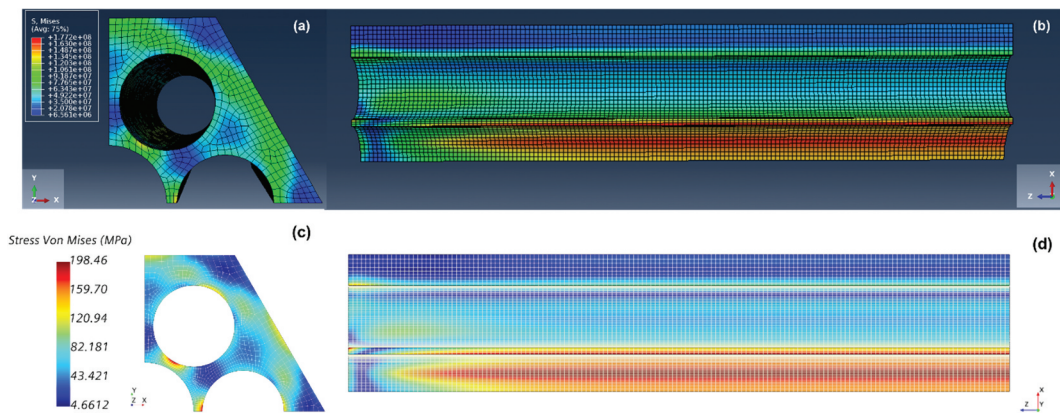


Fig. 14. Von Mises stress distribution with the heating power of 317 W/cartridge heater, (left) top and (right) side view of the hex block [(a) ABAQUS and (b) STAR-CCM+].

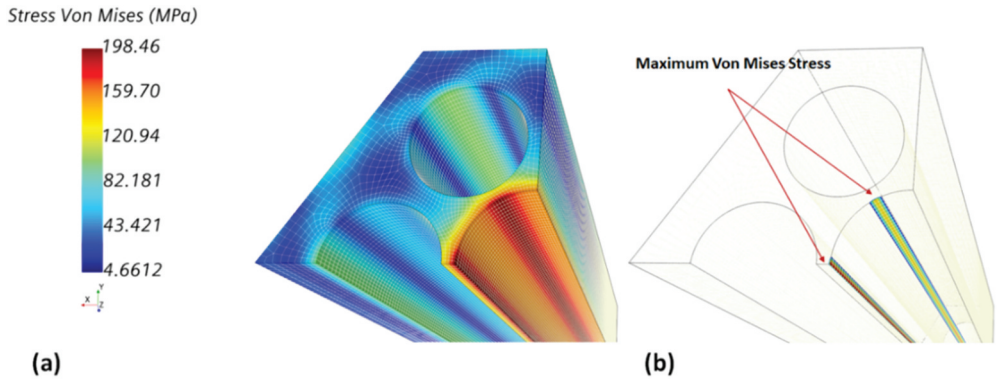


Fig. 15. Location of the maximum Von Mises stress in the hex block.

changing the power of the cartridge heaters and observing the variation of the range of the temperature and the corresponding thermal stress. The heating powers of 100% (i.e., 317 W per cartridge heater), 50% (158.5 W per cartridge heater), and 25% (79.25 W per cartridge heater) were applied while the other parameters and conditions remained the same. Table II summarizes the results from ABAQUS and STAR-CCM+ for the different power levels; both temperatures and Von Mises stress magnitudes linearly increase with the increasing power levels. The range of temperatures of ABAQUS and STAR-CCM+ are almost the same, although the range of the stress is higher in STAR-CCM+ in every case. The differences in the results are quantified by relative error calculated for STAR-CCM+'s results with the reference of ABAQUS's and summarized in Table III. The temperature calculations show a good match between both software; the minimum and maximum temperature differences are all less than 0.3%. As the energy equation for the test section contains only heat conduction, the temperature results should be close to each other, as expected. On the other hand, the Von Mises stresses display larger differences between these two codes. For minimum stresses, the results from STAR-CCM+ always have lower values, while for maximum values, the results from STAR-CCM+ have

slightly larger values. This indicates that STAR-CCM+ will tend to predict higher stresses than ABAQUS. Mesh sensitivity could be a potential cause for the Von Mises stress deviations and will be investigated in future studies.

IV. INSTRUMENTATION AND SENSORS

Some information, such as the permanent mechanical deformations caused by plastic strain or thermal creep, can be gleaned from posttest examination of microreactor components subjected to electrical heating and temperature gradients that are representative of expected conditions during nuclear operation. However, the major benefits to performing electrically heated experiments, besides not having to work with nuclear fuel, reactor constraints, and activated materials, are the ability to incorporate more detailed instrumentation during the tests and better control the environmental conditions. Nonnuclear experiments will provide detailed distributions of thermomechanical parameters (i.e., temperature and strain) and quantify the fundamental limitations of microreactor components and systems, including the heat

TABLE II
Temperature and Stress Range for the Hex Block with the Different Heating Powers

Tool	Power Level	Temperature (°C)		Von Mises Stress (MPa)	
		Minimum	Maximum	Minimum	Maximum
ABAQUS	25%	653.9	669.0	1.7	45.1
	50%	658.7	687.9	3.3	89.5
	100%	665.5	725.3	6.6	177.2
STAR-CCM+	25%	653.5	669.0	1.1	48.6
	50%	657.0	687.8	2.3	96.6
	100%	664.0	725.0	4.5	190.8

TABLE III
Percent Difference of Temperature and Von Mises Stress Comparison Between ABAQUS and STAR-CCM+

Power Level	Percent Difference in Temperature		Percent Difference in Stress	
	Minimum	Maximum	Minimum	Maximum
25%	-0.05	-0.01	-31.00	7.70
50%	-0.11	-0.02	-30.73	8.03
100%	-0.22	-0.03	-31.59	7.70

rejection capabilities of heat pipes and advanced heat exchangers.

Instrumentation with a low technical readiness level will first be tested/demonstrated in SPHERE before being utilized in MAGNET. SPHERE is designed to test the heat rejection capabilities of small monolithic stainless steel test articles that include a single heat pipe surrounded by six electrically heated cartridge heaters. A gas-gap calorimeter surrounds the cooled end of the heat pipe. This calorimeter includes flowing water and is instrumented with a flow meter and inlet and outlet temperature sensors to quantify the heat rejected to the coolant. Combining the measured heat rejection and input electrical power enables measurement of the power that dissipates through the heat pipe as a function of operating temperature. The test articles are contained inside a quartz tube that allows control of the internal atmosphere and visualization of the internal components. In addition, feedthroughs at the top of the tube allow for passing instrumentation and electrical power leads in and out of the facility. All SPHERE tests will include electrical power leads for energizing the cartridge heaters and thermocouples for monitoring temperature throughout the facility. Thermocouples are also being embedded directly within the test articles and inside heat pipes to provide a more detailed mapping of temperatures. To provide an even-higher degree of spatial resolution, spatially distributed fiber optic temperature sensors based on optical frequency domain reflectometry, are included inside the test articles and heat pipes. During steady-state operation at constant power, rapid increases in temperature or the temperature difference between the evaporator entrance and exit will serve as indicators that the heat pipe has exceeded a thermal limitation based on various phenomena such as sonic velocity at the evaporator exit, capillary flow within the wick, entrainment counter flow, or boiling and local dryout near the wall.

The SPHERE and MAGNET facilities allow for testing the performance of a single heat pipe and an array of heat pipes, respectively, under expected

thermal stresses. The embedded spatially distributed fiber optic temperature sensors and thermocouples will provide a detailed mapping of temperatures to determine expected thermal strains. In addition, spatially distributed fiber optic strain sensors are being embedded within the test articles in an attempt to directly monitor local strains. Understanding these strains is critical to ensuring that the heat pipes and electrical heaters (simulating fuel rods) do not debond from the test articles. If this were to occur, there is concern that a single failure could increase the heat rejected to surrounding heat pipes, as well as the temperature gradients throughout the monolith, and ultimately lead to a cascading failure event. A seven-hole test article has been fabricated with two Type K thermocouples directly embedded in its walls using ultrasonic additive manufacturing^{16,18} (UAM). The test article also includes embedded, spatially distributed fiber optic strain sensors mentioned in Refs. 19, 20, and 21 and cavities for inserting spatially distributed fiber optic temperature sensors mentioned in Refs. 22 and 23. Figure 16 shows pictures of the sensor-embedding process and the final seven-hole test article after sensor embedding and post-embedding machining. The sensors survived the embedding process and are currently being characterized at ORNL prior to being sent to INL for testing in SPHERE.

In addition to the embedded temperature sensors, multiple-segment sensors offer the ability to measure several discrete locations along their lengths while only requiring a single lead into the experiment. Distributed temperature sensors that have been developed under the Nuclear Energy Enabling Technologies Advanced Sensors and Instrumentation Program include distributed thermocouples, distributed optical fiber-based temperature sensors, and distributed ultrasonic thermometers (UTs) that will be deployed to demonstrate performance in these test beds to provide guidance for their use in specific temperature

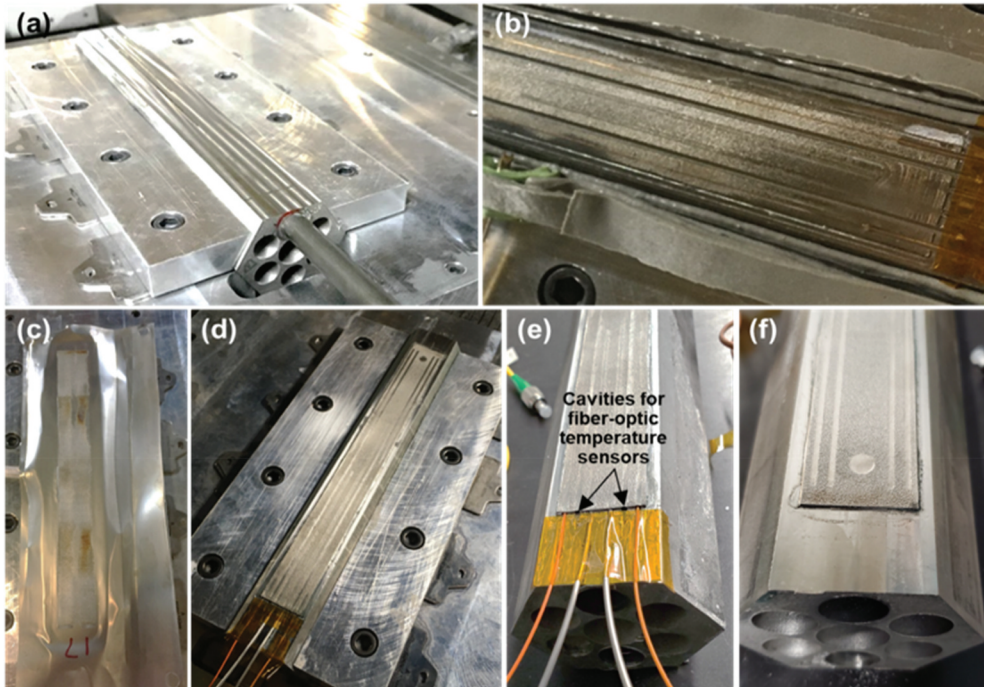


Fig. 16. Pictures of a stainless steel mini hex block during sensor embedding showing (a) the hex block for SPHERE during its manufacturing (drilling) process, (b) UAM layering for embedding the sensors, (c) completion of the UAM layering process, (d) post-embedding machining, and (e) and (f) the finished part with embedded sensors installed.

ranges, responses, resistance to electro-motive force, robustness, etc.

A commercially fabricated Type K multipoint thermocouple was procured from Idaho Laboratories Corporation. It uses ten thermocouple junctions. The first thermocouple, beginning at the tip of the mineral-insulated, metal-sheathed cabling is followed by others at 7-in. spacing inside of a 0.118-in.-o.d. stainless steel sheath. The ten-point thermocouple has been installed and successfully evaluated in SPHERE, as shown in Fig. 17, for initial startup tests up to approximately $740^{\circ}\text{C} \pm 5.5^{\circ}\text{C}$ (Ref. 4).

A multipoint UT that was previously developed for irradiation testing experiments has been fabricated.²⁴ The UT uses temperature-dependent changes in the speed of sound of a metallic waveguide to measure temperature; the temperature is correlated to the delay time of acoustic pulses propagating along the waveguide. Thus, the measured temperature is the average temperature between the measurement nodes. The UT was fabricated with a 0.084-in. o.d. with eight temperature measurement zones. The nodes are located at 22, 28, 35, 48, 60, 82, 89, and 96 in. from the transducer. The UT was fabricated with a stainless steel sheath and molybdenum waveguides and can be operated up to at least $1000^{\circ}\text{C} \pm 10^{\circ}\text{C}$.

The two types of optical fiber-based sensors chosen for deployment in the SPHERE and MAGNET facilities

have been previously demonstrated in-pile in the Transient Reactor Test Facility reactor. Each sensor type has benefits: the optical frequency domain reflectometry (OFDR) sensor has a spatial resolution down to 0.03 in. while the fiber Bragg grating (FBG) sensor allows for measurements up to 1 kHz. The FBG sensor is stable to higher temperatures than the OFDR without adaptive reference techniques to account for increased oxygen mobility at higher temperatures,²⁴ femtosecond FBGs are better suited for temperature sensing beyond $\sim 700^{\circ}\text{C}$. The femtosecond FBG sensor, shown in Fig. 18, was fabricated with nine discrete gratings spaced 9.84 in. apart that are intended to be operated up to 650°C with minimal drift, with the potential to operate up to 1000°C expected before failure.²⁵ Alternatively, the OFDR can be used for spatially distributed temperature measurements using the intrinsic Rayleigh backscatter in unaltered pure-silica core fiber with a fluorine-doped cladding. Both fibers have been installed in 0.063-in.-o.d. \times 0.010-in. wall stainless steel tubes to aid in installation and removal. In this configuration, the sensors will be sensitive to temperature but will not respond to strain in the experimental components.

In addition to fiber optic strain sensors and traditional strain gauges, the quartz tube that is used as a pressure boundary in SPHERE could allow for the



Fig. 17. Ten-point Type K thermocouple in SPHERE.

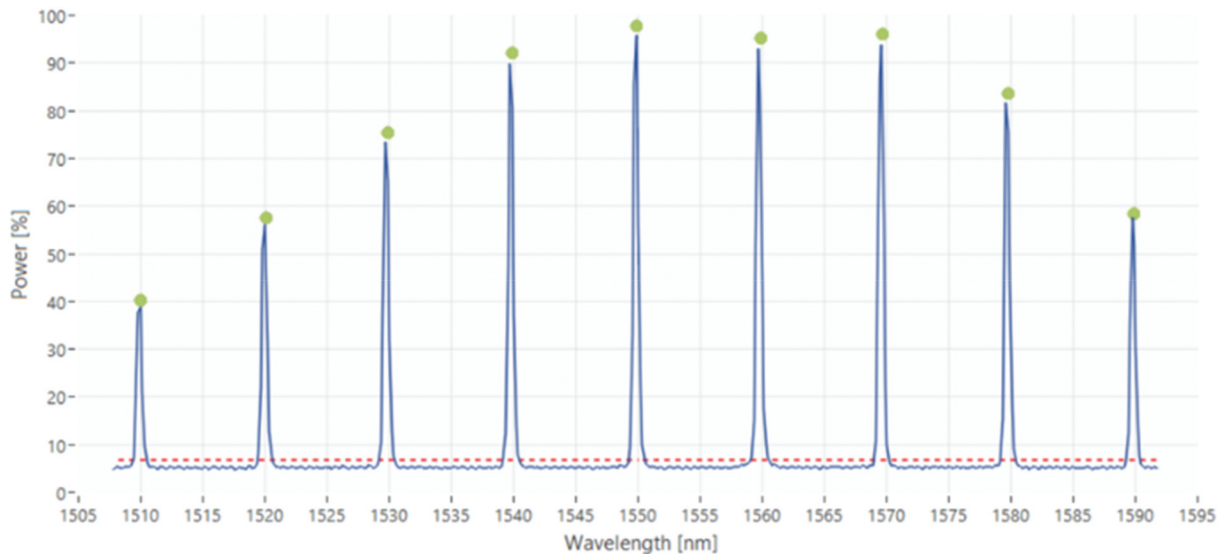


Fig. 18. Spectral response of a FBG sensor fabricated for deployment in SPHERE and MAGNET for distributed temperature measurement.

use of noncontact optical techniques for characterizing local strains. Techniques such as DIC are being evaluated for potential deployment in SPHERE. DIC has shown itself to be a very attractive technique for measuring strain and deformation at high spatial resolution as a noncontact, imager-based technique that can potentially be used to measure strain and deformation in two or three dimensions. In a typical DIC measurement, a speckle pattern is applied to the structure under test and is observed as it undergoes deformation

loading using imagers. MAGNET has optical windows that can provide the required optical access for DIC, which can measure the full-field deformation of the core block, along with all other embedded and spatially distributed sensors that can be deployed within MAGNET experiments. This allows for testing an array of heat pipes and could be used to evaluate a potential cascading heat pipe failure scenario.

Digital image correlations involves the use of one or more imagers for measuring the deformation of

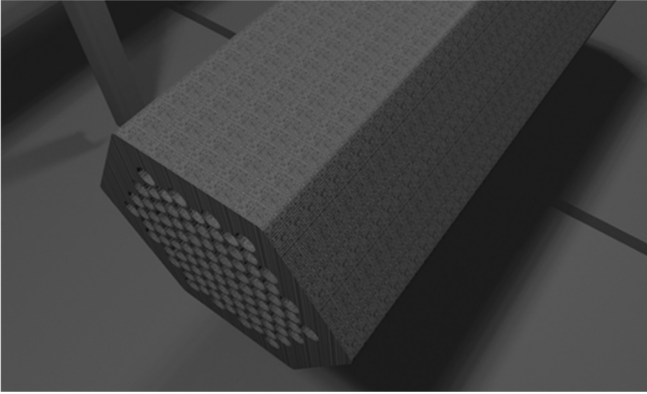


Fig. 19. Simulation of 37-hole core block with speckle pattern for the MAGNET facility.

structures. Its techniques can achieve subpixel resolution. This makes it attractive in applications that allow for line-of-sight viewing of the structure of interest because they allow the capture of deformation information with a very high spatial resolution. DIC would not be practically possible to achieve similar spatial resolution with traditional strain measurement techniques, such as strain gauges. It typically involves placing a high-contrast random speckle pattern coating on the test article of interest.²⁶ In the case of the microreactor core block, the speckle pattern will be applied to the test article using high-temperature paint.

It is currently planned that the imagers using DIC will observe the test article through the viewport located on the top of the MAGNET facility and perhaps also through the viewports on the sides of the MAGNET facility.

It is important to match the size of the random speckles such that they take up roughly 5 to 10 pixels in the image plane to maximize spatial resolution. The team is currently making use of computer graphics simulations (Fig. 19) to estimate the proper size of the speckle pattern given the MAGNET facility viewport locations that can accommodate the imagers.

V. CONCLUSIONS

The current work provides a summary of selected experimental capabilities being developed to support nonnuclear demonstration of microreactors under the DOE MRP. The primary experimental hardware capabilities currently under development focus on nonnuclear thermal and integrated systems testing and test articles to perform experiments. Specifically, this includes SPHERE and MAGNET. State-of-the-art instrumentation and sensors are being used to obtain

detailed maps of temperature and the resulting differential thermal strains. In addition, spatially distributed fiber optic strain sensors are being embedded within the test articles in an attempt to directly monitor local strain to inform the applied loading and potential failure modes of monolithic stainless steel core blocks. Data generated from these experiments will support industry and other DOE programs. These data will be made available to researchers and developers for a range of testing purposes to further improve models and the understanding of individual components and the system as a whole. Additionally, a selection of modeling approaches was discussed that can support these experimental capabilities, including heat pipe models and thermal-structural analysis.






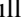




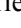
Acknowledgments

The work submitted for this special issue was supported by the DOE Office of Nuclear Energy under the Advanced Reactor Technology portfolio's MRP. The content represents ongoing efforts by the MRP to enable accelerated development and demonstration of microreactor technology.

Disclosure Statement

No potential conflict of interest was reported by the authors.

ORCID

P. Sabharwall  <http://orcid.org/0000-0003-2567-205X>
 J. L. Hartvigsen  <http://orcid.org/0000-0002-9320-5552>
 J. Yoo  <http://orcid.org/0000-0001-8439-7196>
 S. Qin  <http://orcid.org/0000-0002-2850-0387>
 M. Song  <http://orcid.org/0000-0002-8269-1452>
 D. P. Guillen  <http://orcid.org/0000-0002-7718-4608>
 T. Unruh  <http://orcid.org/0000-0003-2417-9060>
 J. E. Hansel  <http://orcid.org/0000-0001-6782-5275>
 J. Gehin  <http://orcid.org/0000-0001-8337-9551>
 H. Trellue  <http://orcid.org/0000-0003-2051-0852>
 C. M. Petrie  <http://orcid.org/0000-0003-1167-3545>

References

1. J. KENNEDY et al., "Special Purpose Application Reactors: System Integration Decision Support," INL/EXT-18-51369, Idaho National Laboratory (Sep. 2018); <https://doi.org/10.2172/1475413>.

2. “DOE Microreactor Program,” Gateway for Accelerated Innovation in Nuclear (GAIN); <https://gain.inl.gov/SitePages/MicroreactorProgram.aspx> (current as of July 2021).
3. P. R. McCLURE et al., “Database of Previous Research Supporting Microreactor Designs,” INL/EXT-18-51298, Idaho National Laboratory (Sep. 2018).
4. P. SABHARWALL et al., “SPHERE Assembly and Operation Demonstration,” INL/EXT-20-60782, Idaho National Laboratory (2020); <https://gain.inl.gov/MicroreactorProgramTechnicalReports/Document-INL-EXT-20-60782.pdf> (current as of Aug. 23, 2021).
5. “C30,” Capstone Green Energy Corporation; <https://www.capstonegreenenergy.com/products/energy-conversion-products/capstone-microturbines/c30> (current as of June 28, 2021).
6. S. A. WRIGHT et al., “Closed Brayton Cycle Power Conversion Systems for Nuclear Reactors,” SAND2006-2518, Sandia National Laboratories (2006); <https://doi.org/10.2172/1177051>.
7. D. P. GUILLEN and D. S. WENDT, “Integration of a Microturbine Power Conversion Unit in MAGNET,” INL/EXT-20-57712, Idaho National Laboratory (Aug. 2020).
8. D. P. GUILLEN and D. S. WENDT, “Technical Feasibility of Integrating a Modified Power Conversion Unit into a Non-nuclear Microreactor Testbed,” *Int. J. Energy Res.*, **45**, 8, 12325 (2021); <https://doi.org/10.1002/er.6517>.
9. J. YOO et al., “Modeling and Analysis Support for High Temperature Single Heat Pipe Experiment: Current Status and Plan,” INL/EXT-21-61961, Idaho National Laboratory (2021).
10. J. YOO et al., “A Conduction-Based Heat Pipe Model for Analyzing the Entire Process of Liquid-Metal Heat Pipe Startup,” *Proc. 19th Int. Topl. Mtg. on Nuclear Reactor Thermal Hydraulics (NURETH-19)*, March 6–11, 2022.
11. A. FAGHRI et al., “A Study of High-Temperature Heat Pipes with Multiple Heat Sources and Sinks: Part I—Experimental Methodology and Frozen Startup Profiles,” *J. Heat Transfer*, **113**, 4, 1003 (1991); <https://doi.org/10.1115/1.2911193>.
12. Y. CAO and A. FAGHRI, “A Numerical Analysis of High-Temperature Heat Pipe Startup from the Frozen State,” *J. Heat Transfer*, **115**, 1, 247 (1993); <https://doi.org/10.1115/1.2910657>.
13. J. E. HANSEL et al., “Sockeye: A One-Dimensional, Two-Phase, Compressible Flow Heat Pipe Application,” *Nucl. Technol.*, **207**, 7, 1096 (2021); <https://doi.org/10.1080/00295450.2020.1861879>.
14. R. S. REID, J. T. SENA, and A. L. MARTINEZ, “Sodium Heat Pipe Module Test for the SAFE-30 Reactor Prototype,” *AIP Conf. Proc.*, **552**, 1, 869 (2001); <https://doi.org/10.1063/1.1358021>.
15. H. TRELLE et al., “Microreactor Agile Nonnuclear Experiment Testbed Test Plan,” LA-UR-20-20824, Los Alamos National Laboratory (2019); <https://doi.org/10.2172/1595649>.
16. C. M. PETRIE and N. D. B. EZELL, “Demonstrate Embedding of Sensors in a Relevant Microreactor Component,” ORNL/SPR-2020/1742, Oak Ridge National Laboratory (2020); <https://doi.org/10.2172/1720216>.
17. S. QIN et al., “Code-to-Code Benchmark Study for Thermal Stress Modeling and Preliminary Analysis of the High-Temperature Single Heat Pipe Experiment,” *Proc. 19th Int. Topl. Mtg. on Nuclear Reactor Thermal Hydraulics (NURETH-19)*, March 6–11, 2022.
18. A. HEHR et al., “Five-Axis Ultrasonic Additive Manufacturing for Nuclear Component Manufacture,” *J. Miner. Met. Mater. Soc.*, **69**, 485 (2017); <https://doi.org/10.1007/s11837-016-2205-6>.
19. C. M. PETRIE and N. SRIDHARAN, “In Situ Measurement of Phase Transformations and Residual Stress Evolution During Welding Using Spatially Distributed Fiber-Ptotic Strain Sensors,” *Meas. Sci. Technol.*, **31**, 125602 (2020); <https://doi.org/10.1088/1361-6501/aba569>.
20. C. M. PETRIE et al., “Embedded Metallized Optical Fibers for High Temperature Applications,” *Smart Mater. Struct.*, **28**, 055012 (2019); <https://doi.org/10.1088/1361-665X/ab0b4e>.
21. C. M. PETRIE et al., “High-Temperature Strain Monitoring of Stainless-Steel Using Fiber Optics Embedded in Ultrasonically Consolidated Nickel Layers,” *Smart Mater. Struct.*, **28**, 085041 (2019); <https://doi.org/10.1088/1361-665X/ab2a27>.
22. T. W. WOOD et al., “Evaluation of the Performance of Distributed Temperature Measurements with Single-Mode Fiber Using Rayleigh Backscatter up to 1000°C,” *IEEE Sens. J.*, **14**, 1, 124 (2014); <https://doi.org/10.1109/JSEN.2013.2280797>.
23. D. C. SWEENEY, A. M. SCHRELL, and C. M. PETRIE, “An Adaptive Reference Scheme to Extend the Functional Range of Optical Backscatter Reflectometry in Extreme Environments,” *IEEE Sens. J.*, **21**, 498 (2020); <https://doi.org/10.1109/JSEN.2020.3013121>.
24. J. E. DAW, L. HONE, and K. WOODBURY, “Testing of an Ultrasonic Thermometer Developed at the Idaho National Laboratory,” *Proc. 2021 IEEE Int. Instrumentation and Measurement Technology Conf. (I2MTC)*, May 17–20, 2021, p. 1 (2021); <https://doi.org/10.1109/I2MTC50364.2021.9459867>.
25. D. C. GROBNIC et al., “Long-Term Thermal Stability Tests at 1000°C of Silica Fibre Bragg Gratings Made with Ultrafast Laser Radiation,” *Meas. Sci. Technol.*, **17**, 1009 (2006); <https://doi.org/10.1088/0957-0233/17/5/S12>.
26. T. THAI et al., “Importance of Exposure Time on DIC Measurement Uncertainty at Extreme Temperatures,” *Exp. Tech.*, **43**, 261 (2019); <https://doi.org/10.1007/s40799-019-00313-3>.